Atmos. Meas. Tech., 3, 947–958, 2010
www.atmos-meas-tech.net/3/947/2010/
doi:10.5194/amt-3-947-2010

Atmospheric Measurement Techniques

Total column CO_2 measurements at Darwin, Australia – site description and calibration against in situ aircraft profiles

N. M. Deutscher[1], D. W. T. Griffith[1], G. W. Bryant[1,*], P. O. Wennberg[2,3], G. C. Toon[4], R. A. Washenfelder[3,], G. Keppel-Aleks[3], D. Wunch[2,3], Y. Yavin[2], N. T. Allen[5], J.-F. Blavier[4], R. Jiménez[5,6], B. C. Daube[5,6], A. V. Bright[5,6], D. M. Matross[5,6,***], S. C. Wofsy[5,6], and S. Park[5,6]**

[1]School of Chemistry, University of Wollongong, Northfields Ave, Wollongong, NSW, 2522, Australia
[2]Division of Geological and Planetary Sciences, California Institute of Technology, 1200 E. California Boulevard, Pasadena, CA, 91125, USA
[3]Division of Engineering and Applied Science, California Institute of Technology, 1200 E. California Boulevard, Pasadena, CA, 91125, USA
[4]Jet Propulsion Laboratory, California Institute of Technology, 4800 Oak Grove Drive, Pasadena, CA, 91109, USA
[5]School of Engineering and Applied Sciences, Harvard University, Cambridge, MA, 02138, USA
[6]Department of Earth and Planetary Sciences, Harvard University, Cambridge, MA, 02138, USA
[*]now at: Centre for Organic Electronic, University of Newcastle, NSW, Australia
[**]now at: Chemical Sciences Division, Earth System Research Laboratory, NOAA, 325 Broadway St, Boulder, CO, 80305, USA
[***]now at: Sustainable Market Strategies Group, KEMA Inc, Oakland, CA, USA

Received: 3 March 2010 – Published in Atmos. Meas. Tech. Discuss.: 17 March 2010
Revised: 26 May 2010 – Accepted: 7 July 2010 – Published: 19 July 2010

Abstract. An automated Fourier Transform Spectroscopic (FTS) solar observatory was established in Darwin, Australia in August 2005. The laboratory is part of the Total Carbon Column Observing Network, and measures atmospheric column abundances of CO_2 and O_2 and other gases. Measured CO_2 columns were calibrated against integrated aircraft profiles obtained during the TWP-ICE campaign in January–February 2006, and show good agreement with calibrations for a similar instrument in Park Falls, Wisconsin. A clear-sky low airmass relative precision of 0.1% is demonstrated in the CO_2 and O_2 retrieved column-averaged volume mixing ratios. The 1% negative bias in the FTS X_{CO_2} relative to the World Meteorological Organization (WMO) calibrated in situ scale is within the uncertainties of the NIR spectroscopy and analysis.

Correspondence to: N. M. Deutscher
(ndeutsch@uow.edu.au)

1 Introduction

Carbon dioxide in the atmosphere is the most important contributor to positive radiative forcing responsible for the enhanced greenhouse effect (Forster et al., 2007). To better understand and manage CO_2 emissions, estimates of source and sink strength and variability are required on at least regional scales. In the past, these regional strengths and patterns of surface exchange across the globe have been quantified via a combination of in situ CO_2 measurements from a global network of surface sites (GLOBALVIEW-CO_2), and inverse modeling studies (Gurney et al., 2002). Despite the high precision and accuracy of the in situ measurements, this approach exhibits a high variability of source/sink distributions across different transport models (Gurney et al., 2003), particularly when attempting to constrain regions on a small spatial scale. Errors in modeling transport are a contributing factor to the varying results between models; however errors are also introduced due to rectifier effects, which arise because the surface fluxes are seasonally and diurnally correlated with vertical transport (Denning et al., 1996; Gurney et al., 2002). Higher surface concentrations occur at night-time and in winter due to CO_2 build up in a shallow planetary

boundary layer (PBL) resulting from decreased convective mixing. The effect of vertical transport model errors on inverse estimates of CO_2 fluxes has been discussed by Gerbig et al. (2008).

Vertical column measurements of CO_2 are less susceptible to these types of sampling bias as they integrate over the entire vertical column rather than simply sampling in the PBL. Column measurements can therefore reduces vertical-transport-induced variability compared to surface data, though at the disadvantage of being less sensitive than in situ measurements to surface sources and sinks. Column measurements can therefore complement the existing in situ network; however, high precision in the column measurements is required for low variability sites, such as those in the Southern Hemisphere, in order to determine meaningful seasonal and spatial patterns (Rayner and O'Brien, 2001). Simulations have confirmed their potential for constraining the global carbon balance if obtained with suitable precision and accuracy (e.g. precision better than 2.5 µmol mol^{-1} for monthly average column data with global coverage with a $8^\circ \times 10^\circ$ footprint) (Rayner and O'Brien, 2001). Particular care must be taken, however, with systematic biases, which must be limited to a few tenths of a µmol mol^{-1} (Chevallier et al., 2007).

The Total Carbon Column Observing Network (TCCON) (http://www.tccon.caltech.edu; Wunch et al., 2010a) is a network of ground-based solar Fourier Transform Spectrometers (FTS) operating in the near infrared (NIR) spectral region, focused on providing highly accurate and precise column measurements of CO_2, as well as simultaneously measuring O_2, CH_4, H_2O, HDO, HF, CO and N_2O and other species. The column data resulting from the site considered here and sites with similar setups can be used not only for validation of satellites, but also in atmospheric inversion modeling studies. Quantification of biases and errors is extremely important for inversion studies, so calibration and subsequent quantification of precision and accuracy of the column measurements is important for their use in this application. Column measurements are especially important in the tropics, as convection is consistently strong, and as a result flux signals are only weakly seen in surface measurements (Gloor et al., 2000; Rayner and O'Brien, 2001). The importance of tropical column measurements in constraining regional flux estimates has previously been emphasized in modeling studies (Gloor et al., 2000; Olsen and Randerson, 2004; Rayner and O'Brien, 2001). The TCCON can potentially provide these data.

By measuring the same quantities (i.e. column abundances) in the same spectral regions as satellite-borne instruments such as the Orbiting Carbon Observatory (OCO) (Crisp et al., 2004), the Greenhouse Gases Observing Satellite (GOSAT) (Inoue et al., 2006) and the SCanning Imaging Absorption SpectroMeter for Atmospheric CHartographY (SCIAMACHY) (Bovensmann et al., 1999), TCCON will be able to provide a definitive validation and calibration of the satellite products. The global network of sites comprising TCCON will be particularly useful for determining and calibrating spatial and temporal variation in the satellite products. A global network is necessary to provide satellite validation over a range of latitudes, surface types, environments and airmasses.

This paper describes the dedicated solar observatory deployed to Darwin, Australia (12.425 S, 130.891 E) in August 2005. The observatory currently is the only continuously operating solar FTS located within the tropics, making it crucial for providing data to constrain this important region, as well as to provide calibration and validation of satellite data over the tropics. Constraining regional-scale source and sink strengths in the tropics is difficult because there are limited CO_2 measurements in this region. Quantifying tropical CO_2 sources and sinks is important because of carbon stocks in tropical rainforests, deforestation, tropical wetlands, the unique presence of savannahs, and the large contribution from regular biomass burning. Darwin has a very distinct climatic pattern – a monsoonal wet season from December to March, a dry season from May to September, and transitions in between these times.

In this paper Sect. 2 describe the instrumentation, Sect. 3 the measurement site and Sect. 4 introduces the data analysis. In Sect. 5 we outline the calculation of total column mole fraction and investigate the reproducibility of these measurements in Sect. 6. Section 7 presents the calibration of atmospheric CO_2 columns to the global reference scale via comparison to integrated in situ aircraft profiles obtained during the Tropical Warm Pool – International Cloud Experiment (TWP-ICE) in January – February 2006. Section 8 contains a discussion of the errors. This is followed by the summary and conclusions, and Appendix A contains a method to correct for airmass dependent effects.

2 Instrumentation

The solar observatory was assembled at the California Institute of Technology (Caltech), and shipped to Darwin, Australia in 2005. The observatory is very similar to that detailed by Washenfelder et al. (2006), who describe the first dedicated TCCON solar observatory deployed to Park Falls, Wisconsin. In summary, a Bruker IFS 125/HR FTS (Bruker Optics, Germany) is mounted inside a customized $6.1 \times 2.4 \times 2.6$ m shipping container. The spectrometer has two room-temperature NIR detectors, an indium gallium arsenide (InGaAs – 3800 – 12 000 cm^{-1}) and a silicon diode (Si – 9500 – 30 000 cm^{-1}) which operate in simultaneous dual acquisition mode with a 10,000 cm^{-1} dichroic filter and calcium fluoride (CaF_2) beamsplitter. A red filter limits the Si spectra to 15 600 cm^{-1} to avoid aliasing. Atmospheric column abundances of CO_2, O_2, CH_4, H_2O, HDO, HF, CO and N_2O can be retrieved from the NIR spectra. A Bruker Optics solar tracker is mounted on the roof of the container and

protected by an astronomy dome (ROBODOME™, Technical Innovations Inc., Gaithersburg, Maryland). The tracker directs the solar beam through a CaF_2 window in the roof of the container and onto a folding mirror below, where it is then reflected into the spectrometer. A pickoff mirror directs a small fraction of the beam to a Si quadrant detector that controls the active solar tracking. Scans are routinely collected over optical path differences of −5 cm to 45 cm, with a mirror speed of 0.633 cm s^{-1} (fringe rate 10 kHz, sample rate 20 kHz) resulting in a collection time of 76 s for a single scan.

Daily operation of the container is fully automated. A weather station monitoring temperature, relative humidity, solar radiation, presence of rain, leaf wetness and pressure is also mounted on the roof of the container. Housekeeping data, including meteorological parameters, are logged continuously at a frequency of 1Hz. Active solar tracking and spectral collection are initiated when the solar intensity measured at the quadrant detector is greater than ∼45 W m^{-2}. The pressure as measured with a Setra Systems Inc. Model 270 pressure transducer is periodically calibrated against a mercury manometer mounted inside the container. The precision of the pressure transducer is approximately 0.03% (0.3 hPa).

The differences from the Park Falls setup detailed in Washenfelder et al. (2006) are the inclusion of a leaf wetness sensor on the weather station (now also installed at Park Falls) and the increased fringe rate from 7.5 kHz to 10 kHz (which has since been changed back to 7.5 kHz to reduce data volume) and hence reduced spectral collection time of 76 s rather than 105 s. On 29 September 2005, the method of data collection was changed from the normal AC recording to DC acquisition mode. Collecting DC interferograms enables correction for source brightness fluctuations during each scan that occur due to changing thin cloud and aerosol cover. The switch to DC acquisition improves the reproducibility of column-average dry-air mole fraction (X_{CO_2}) under partly cloudy conditions, as well as the number of usable spectra obtained (Keppel-Aleks et al., 2007).

In addition to the room-temperature InGaAs and Si-diode detectors, a liquid nitrogen cooled indium antimonide (InSb) detector (2000–6500 cm^{-1}) is installed. Spectra are collected with this detector at times of biomass burning that occur during the dry season in the savannahs across tropical Australia. The additional spectral coverage provided by the InSb detector results in the ability to simultaneously monitor biomass burning species including CO, HCN, C_2H_6, C_2H_2 and H_2CO (Paton-Walsh et al., 2010), although these gases are not the subject of this paper.

The instrument has operated almost continuously since installation, however short data gaps of up to one month have occurred due to a battery failure in April 2006 and computer failure in June 2007. Aside from this, the major problem encountered has been degradation of the external gold-coated solar tracker mirrors, which have been replaced on two occasions, in early December 2005 and early November 2006. The mirror coating degradation causes a progressive reduction in light throughput, resulting in decreased signal-to-noise ratio, and consequently, measurement reproducibility. In the first two years of operation, data were collected on 588 days, with an average of 250 spectra per day during the dry season.

3 Measurement site

The laboratory is located at the Department of Energy (DoE) Tropical Western Pacific (TWP) Atmospheric Radiation Measurement (ARM) site, located adjacent to the Australian Bureau of Meteorology (BoM) station at Darwin International Airport (12.425 S, 130.89 E, 30 m above sea level). The site is 9 km from the city of Darwin (population 90 000). The airport typically has fewer than 30 incoming and outgoing commercial flights per day plus sporadic military use. Thus interference from aircraft exhaust emissions is minimal, especially as airport peak traffic is after sunset, when solar measurements cannot be collected. The ARM site was chosen because of the existing infrastructure and technical support available, as well as the suite of ancillary measurements available both there and at the BoM site. An in situ FTIR trace gas analyzer similar to that described by Esler et al. (2000a, b) has been in place since February 2007, measuring CO_2, $\delta^{13}C$ in CO_2, CH_4, N_2O and CO at 12 m above ground level.

4 Data analysis

DC corrected spectra are analyzed using GFIT, a non-linear least-squares fitting algorithm developed at the Jet Propulsion Laboratory (G. Toon). A theoretical atmospheric transmittance spectrum is calculated using molecular absorption coefficients, calculated atmospheric ray paths, model assimilated profiles of temperature, pressure and humidity and assumed gas dry-air mole fraction profiles. The temperature, pressure and water vapor profiles are obtained from National Center for Environmental Prediction (NCEP) reanalysis data (Kalnay et al., 1996) provided by the NOAA/ESRL Physical Sciences Division, and interpolated in time and space from six hourly data to local solar noon and site latitude/longitude. The a priori CO_2 profile is based on a model fitted to GLOBALVIEW data. The GFIT forward model calculation uses 70 vertical levels spaced at 1 km intervals to represent the atmosphere. The calculated and measured spectra are compared, and the RMS difference between the two is minimized by iteratively scaling the gas VMR profiles.

CO_2 columns are retrieved in two bands centered at 6228 cm^{-1} ($\nu_1 + 4\nu_2 + \nu_3$) and 6348 cm^{-1} ($2\nu_1 + \nu_2 + 2\nu_3$), from which we use the average column amount. Figure 1a shows a typical pair of simultaneously acquired InGaAs and Si spectra, with (b) an expanded view of the 6228 cm^{-1}

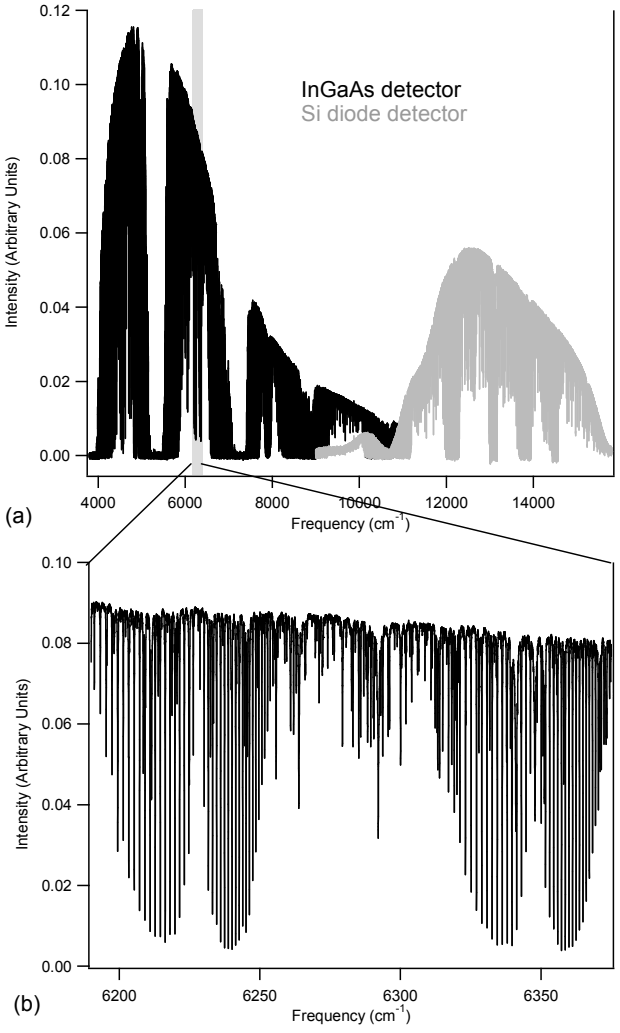

Fig. 1. (a) Typical InGaAs (black) and Si (grey) spectra, obtained simultaneously from Darwin on July 10, 2006. **(b)** Expanded view of the CO_2 6228 cm^{-1} ($\nu_1 + 4\nu_2 + \nu_3$) and 6348 cm^{-1} ($2\nu_1 + \nu_2 + 2\nu_3$) bands from the same spectrum.

and 6348 cm^{-1} CO_2 bands. The O_2 A-band (13070 cm^{-1}), which was to be used for retrievals by the OCO satellite (Crisp et al., 2004), is not used in our analyses. Instead, we use the 7882 cm^{-1} O_2 band, which has the advantage of being collected using the same detector as the two CO_2 bands, and being closer in frequency, so that systematic effects such as instrument lineshape (ILS) errors, zero level offset, and aerosol and cloud scattering will be more similar between the three bands and therefore mostly cancel in the CO_2/O_2 ratio.

The spectral line parameters are based on the HITRAN linelist (Rothman et al., 2005), with improvements to the O_2 7882 cm^{-1} band (Newman et al., 2000; Yang et al., 2005), CO_2 6228 cm^{-1} and 6348 cm^{-1} bands (Toth et al., 2006, 2007), the CH_4 6002 cm^{-1} band (Frankenberg et al., 2008)

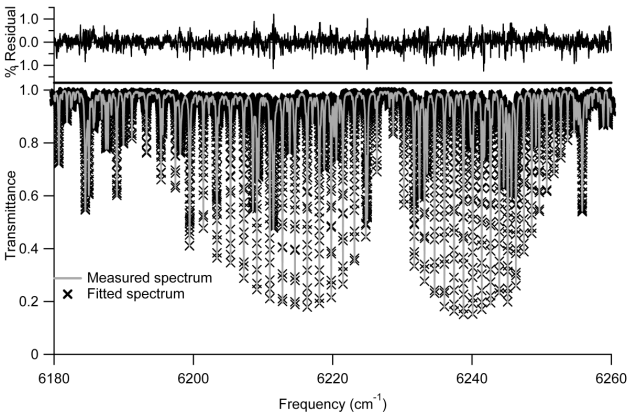

Fig. 2. An example measured (grey) and fitted (black crosses) spectrum in the CO_2 6228 cm^{-1} band, along with the percentage residual difference (black – upper panel) between the two spectra. This particular spectrum was measured on 20 December 2005 at a solar zenith angle of 12 deg.

and H_2O (Toth, 2005), with the addition of hundreds of weak empirically-derived H_2O lines observed in the spectra. A model of collision-induced absorption (CIA) of O_2-O_2 and O_2-N_2 based on laboratory measurements (Smith and Newnham, 2000; Smith et al., 2001) is also included to improve estimation of the continuum in the O_2 7882 cm^{-1} band. The modified linelist is available upon request to Geoff Toon (JPL). An example of a measured spectrum, its calculated fit and the residual difference between them for the CO_2 6228 cm^{-1} band is shown in Fig. 2. The largest residuals are caused by solar features.

5 Calculation of total column mixing ratios

We convert the raw retrieved whole air columns to column-average dry-air mole fractions (DMFs) via Eq. (1) by dividing the vertical column of gas by that of the total dry atmosphere:

$$X_i = \frac{\mathrm{VC}_i}{\frac{P_s}{m_{\mathrm{air}}^{\mathrm{dry}} \cdot \hat{g}} - \mathrm{VC}_{\mathrm{H_2O}} \cdot \frac{m_{\mathrm{H_2O}}}{m_{\mathrm{air}}^{\mathrm{dry}}}} \quad (1)$$

where:

X_i = column-average dry-air mole fraction of gas i
VC_i = vertical column of gas i (molecules cm^{-2})
P_s = surface pressure(mb)
$\hat{g}$ = absorber weighted gravitational acceleration
$m_{\mathrm{air}}^{\mathrm{dry}}$ = molecular mass of dry air (28.964g mol^{-1})
$m_{\mathrm{H_2O}}$ = molecular mass of H_2O (18.02g mol^{-1})

For O_2, we know the atmospheric profile to have a constant dry-air mole fraction of 0.2095. We can therefore rearrange Eq. (1) to yield the relationship (2), which presents the total

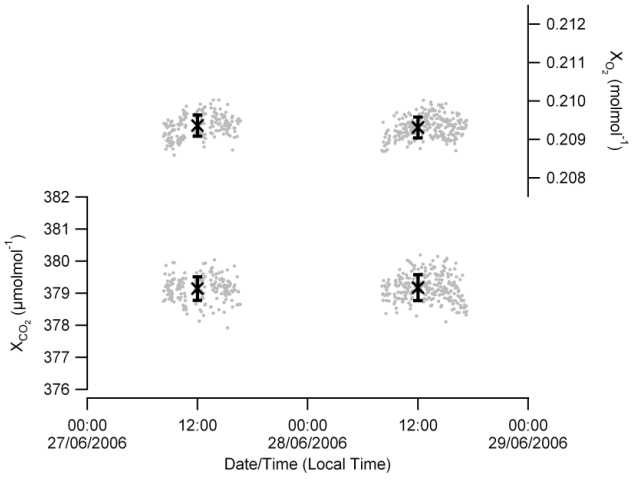

Fig. 3. X_{CO_2} (left axis) and X_{CO_2} (right axis) filtered for solar intensity variation and retrieval error, and corrected for airmass dependence on the 27 and 28 June 2006. The crosses with error bars represent the mean +/− standard deviation of each day's measurements.

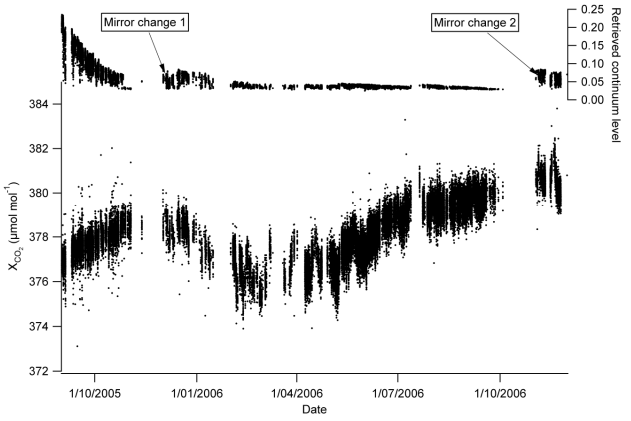

Fig. 4. Time series of X_{CO_2} (left axis) and retrieved continuum level from installation until 1 December 2006. The continuum level is the signal that would be measured in the absence of atmospheric absorption and is therefore independent of gas concentrations and provides an accurate measure of the optical throughput. Mirror replacements occurred in December 2005 and November 2006, as indicated by the arrows on the plot.

dry air column in terms of the vertical column of O_2, rather than pressure. Substituting back into (1) gives Eq. (3), which allows X_i to be calculated using VC_{O_2} from simultaneously acquired spectra. This eliminates systematic errors that are common to species i and O_2, such as those from solar intensity variation and ray path variation due to scattering and solar pointing. We also eliminate site-dependent biases that may arise in the surface pressure and gravity, thereby increasing the measurement accuracy. Systematic errors in X_i may be introduced in the long-term by any variation in retrieved O_2 that does not similarly affect trace gas i.

$$\frac{P_s}{m_{air}^{dry} \cdot g} - VC_{H_2O} \cdot \frac{m_{H_2O}}{m_{air}^{dry}} = \frac{VC_{O_2}}{X_{O_2}} = \frac{VC_{O_2}}{0.2095} \quad (2)$$

$$X_i = \frac{VC_i}{VC_{O_2}} \cdot 0.2095 \quad (3)$$

One of the advantages of Darwin over Park Falls is that the natural variations of X_{CO_2} are much smaller, allowing systematic errors in the data to be more easily identified and quantified. The high range of solar zenith angles and large number of sunny days further helps with this error characterization.

Plots of X_{CO_2} as a function of solar zenith angle reveal ∼1% larger values around noon than sunrise/set. This occurs at all TCCON sites and seasons, even when the true variation of CO_2 is known to be small. This so-called airmass-dependent-artifact is believed to arise from spectroscopic deficiencies and has been corrected in the data presented here. A description of this correction is given in Appendix A, and further detail given by Wunch et al. (2010a).

6 O_2 and CO_2 reproducibility

X_{CO_2} and X_{O_2} are filtered for relative solar intensity variation of less than ten percent during each scan, and retrieval error of less than 0.02 (∼2%) in the calculated profile scale factor. X_{O_2} allows us to ensure the repeatability of the measurements that could otherwise be limited by scattering, ray path variation or the precision of the pressure transducer. For each day of measurements, the percentage standard deviation is calculated to give an indication of the within-day measurement reproducibility (GAW, 2007). Figure 3 shows the retrieved X_{CO_2} and X_{O_2}, along with the daily mean ± standard deviation (crosses and error bars) for two example days, June 27 and 28, 2006. Here the X_{O_2} is calculated via Eq. (1) and scaled to a mean value of 0.2095, but for the remainder of this manuscript the unscaled X_{O_2} is used. On clear sky days such as these (>60 spectra), the reproducibility of X_{CO_2} is better than 0.09% (one standard deviation) and X_{O_2} better than 0.11%. The better reproducibility in X_{CO_2} over X_{O_2} occurs because of the cancellation of errors common to CO_2 and O_2 columns. The clear sky reproducibility of the column measurements is therefore of the order of 0.1%.

The reproducibility of the CO_2 and O_2 retrievals is much better than the RMS uncertainty achieved by the spectral fit, such as that illustrated in Fig. 2. Since the fitted CO_2 windows contain around 100 spectral lines it is possible to achieve a reproducibility in the retrieved columns that is better than the RMS spectral fit. The RMS residual is also affected by systematic effects which are invariant from spectrum-to-spectrum and do not affect the reproducibility of the measurement.

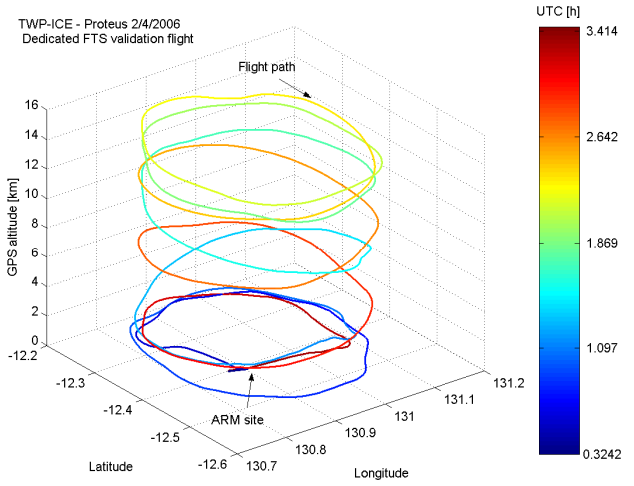

Fig. 5. Trajectory of the 4 February DoE-Proteus flight. The black dot represents the ARM site at which the FTS is located. The color scale shows the progression through time in UT, from blue at take off, through green at the upward spiral completion to red at landing.

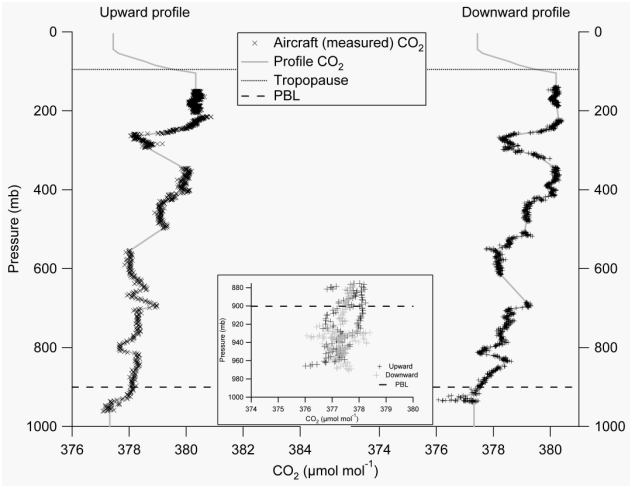

Fig. 6. In situ CO_2 measured through the upward (left) and downward (right) spirals on 4 February 2006. The crosses show the concentrations as measured by the aircraft instrument, while the grey line shows the pressure-binned values used for integrating to obtain the total profile. The PBL and tropopause heights are indicated by the dashed and solid horizontal lines, respectively. The inset shows the aircraft measured CO_2 mixing ratios in the lowest fraction of the profile, along with the PBL height.

A time series of 14 months of X_{CO_2} data is presented in Fig. 4. A seasonal pattern in CO_2 is evident, with peak mole fraction at the start of the monsoon season, followed by rapid uptake due to the onset of plant growth and then a resumption of CO_2 growth from the end of the rainy season. Also shown in this figure is the time series of retrieved continuum level, hence indicating the relative signal levels. A decrease in signal can be seen throughout the time series. Some of the lost signal is regained with replacement solar tracker mirrors in December 2005 and November 2006.

7 Column CO_2 calibration against in situ measurements

We have shown that good reproducibility can be obtained on the solar column CO_2 measurements. In addition to the airmass-dependent biases discussed earlier, there are also systematic biases that are airmass-independent, probably resulting from spectroscopic errors in the integrated band intensities. These are actually easier to deal with because they are invariant. In order to correct for these biases and place these measurements on the same CO_2 scale as used for in situ measurements (Tans et al., 2003), and thus to be able to use them alongside in situ data for satellite validation and inverse modeling, they need to be calibrated against a standard technique on an absolute scale. This requires simultaneous, co-located measurement of CO_2 profiles that are calibrated on the WMO CO_2 scale.

The Tropical Warm Pool International Cloud Experiment aircraft mission (TWP-ICE, January–February 2006) provided the opportunity to perform such calibration against CO_2 profiles measured in situ with the "ER-2" NDIR CO_2 analyzer on board the Proteus aircraft. Simultaneous, co-located CO_2 profiles obtained during this campaign are integrated for comparison with the retrieved FTS column CO_2.

The Harvard University "ER-2" CO_2 instrument is described in detail elsewhere (Daube et al., 2002). Briefly, the instrument is based on a modified NDIR CO_2 analyzer (Li-Cor LI-6251), which measures the light absorption of the sample at 4.26 µm relative to a reference gas of known CO_2 concentration. A Nafion drier and a dry ice trap were added to the instrument for its deployment on Proteus. Dilution by water vapor and wall effects are negligible at the resulting sample dewpoint ($<-60°$ C). Calibrations with reference (zeroing), low- and high-span, and a long-term standard, were performed in flight every 10, 30 and 120 min, respectively. The calibration with a long-term standard ensures flight-to-flight accuracy and precision, which is augmented by ground-based calibrations of the source and instrument tanks before and after the mission. All the calibration gases are traceable to WMO primary standards. The demonstrated (>160 flights) precision and accuracy of the instrument is better than ± 0.1 µmol mol^{-1}. The CO_2 mixing ratio is reported at 0.5 Hz (2 s response time).

During TWP-ICE, CO_2 was measured on Proteus during five flights: 25, 27 and 29 January and 2 and 4 February 2006. These flights were all during the wet or monsoon season. Only the last flight occurred under clear sky conditions, so the comparison uses data from the Feb 4 flight only. The flight consisted of an upward and a downward spiral centered on the ARM site. CO_2 measurements commenced at

00:51 UT (10:21 LT). Figure 5 shows the trajectory of the 4 February flight centered on the observatory. The color scale from red to blue represents the progression through time of the flight.

The total CO_2 vertical column from the in situ aircraft profile is determined by integrating the measured profiles:

$$\mathrm{VC}_{\mathrm{CO}_2} = \int_0^{P_s} \frac{f_{\mathrm{CO}_2}^{\mathrm{dry}} \cdot (1 - f_{\mathrm{H_2O}})}{g(p) \cdot m} dp \quad (4)$$

$$\text{with } m = [m_{\mathrm{H_2O}} \cdot f_{\mathrm{H_2O}} + m_{\mathrm{air}}^{\mathrm{dry}} \cdot (1 - f_{\mathrm{H_2O}})] \quad (5)$$

where:

$f_{\mathrm{CO}_2}^{\mathrm{dry}}(p) =$ dry−air mole fraction of CO_2 (mol mol^{-1});
$f_{\mathrm{H_2O}}(p) =$ mole fraction of H_2O (mol mol^{-1});
$m(p) =$ mean molecular mass of (wet) air
$g(p) =$ gravitational acceleration

This formulation requires measurements of CO_2 and H_2O throughout the vertical profile. The Proteus Harvard instrument provides $f_{\mathrm{CO}_2}^{\mathrm{dry}}$, but there was no reliable co-located measurement of water vapor aboard the Proteus flights. As an alternative, we use humidity data collected using a Vaisala RS92$^{\mathrm{TM}}$ sensor on board a balloon-borne sonde launched from the ARM site that flew between 0845 and 1030 local time on the flight day. These humidity data are corrected using the algorithm presented by Vömel et al. (2007a, b), with a further correction to eliminate solar zenith angle dependence (Hume, 2007). They are then interpolated onto the aircraft pressure grid, and used as $f_{\mathrm{H_2O}}$ in the integration. The contribution of H_2O to the total error budget is small – a systematic error of 5% (the quoted total uncertainty in the Vaisala RS92 for a sounding) in the balloon-borne H_2O concentrations would result in an X_{CO_2} error of 0.03 µmol mol^{-1} (0.008%).

The 4 February airborne spiral (139–961 hPa) covers a large vertical portion of the troposphere. Nevertheless, in order to determine the entire integrated column, it is necessary to extrapolate the CO_2 profile to the lowermost part of the planetary boundary layer (PBL) and to the uppermost part of the troposphere and the stratosphere. This requires formulating some assumptions about the CO_2 profile within these regions of the atmosphere.

The average of five NCEP model runs commencing at different times is used to determine the PBL height for Darwin. The NCEP model runs agree well with the PBL height calculated from the balloon-borne soundings. It is assumed that the PBL is sufficiently well mixed during the time of the flight, so that a constant CO_2 profile is used based on aircraft PBL measurements, and scaled to match the bottom of the profile. In the PBL, $f_{\mathrm{CO}_2}^{\mathrm{dry}}$ is particularly sensitive to spatial variations, due to localized sources/sinks. At these altitudes, the Proteus digressed from the spiral profile to make its landing. The inset in Fig. 6 shows the suite of CO_2 measurements

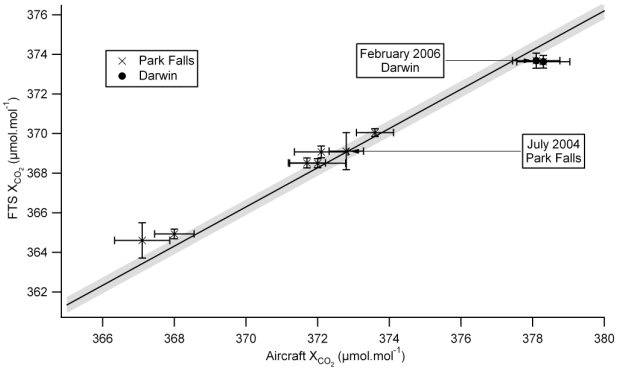

Fig. 7. The retrieved average FTS X_{CO_2} plotted against the aircraft X_{CO_2} for all Darwin and Park Falls profiles. The lines show the best fit to the ratio of each FTS window to all aircraft profiles for Park Falls and Darwin, with each point overlying the best fit line within the uncertainties.

in the PBL from Proteus during the ascent and descent, along with the modeled PBL height. The $f_{\mathrm{CO}_2}^{\mathrm{dry}}$ value varies by approximately ± 1 µmol mol^{-1}, within the error estimate given. The variability is both spatial and temporal, and occurs during the spirals and the preceding and succeeding flight time.

The tropopause height is supplied by NCEP reanalysis. Below the tropopause but above the aircraft ceiling, the free troposphere CO_2 profile is assumed to be equal to the mean profile value measured above 200 hPa. Above the tropopause, a stratospheric model is used to generate the stratospheric CO_2 profile. The model uses time and latitude (and N_2O as internal variable) to determine the age of the air since entering the stratosphere (Andrews et al., 1999; 2001a, b) along with surface measurements of CO_2 at Samoa and Mauna Loa (Boering et al., 1996) to compute stratospheric CO_2 profiles for either the equatorial region ($\sim -5°$ to $+5°$) or mid-latitudes (35° to 55°). To obtain the value at Darwin, a linear interpolation is performed between the equatorial profile at 5° latitude and the profile at 35° latitude to obtain a stratospheric CO_2 profile at 12.425° latitude. The rapid transport of tropical CO_2 to the lower Tropical Tropopause Layer (TTL) has recently been confirmed using CO_2 measurements on the WB-57 during CR-AVE (2006) and on Proteus during TWP-ICE (Park et al., 2007).

Profile values from the Proteus are allocated errors of 0.1 µmol mol^{-1} (1-sigma) in calculating the integrated column error, while all the assumed profile values are assigned error bars of 2 µmol mol^{-1}. The measured (crosses) and extrapolated (lines) portions of the profiles are shown in Fig. 6. The entire profile is weighted by the mean vertically resolved FTS averaging kernel over the period of the overpass and both retrieval windows, before comparing with FTS column retrievals. The method of applying and calculating the averaging kernel is described by Wunch et al. (2010b). The averaging kernel is derived by perturbing the mole fraction

Table 1. Summary of the column average dry-air mole fractions obtained during the intercomparison between the FTS and the in situ instrument on board Proteus.

Profile	Aircraft X_{CO_2}	FTS X_{CO_2}	Number FTS spectra
Upward	378.1 ± 0.7	373.7 ± 0.4	49
Downward	378.3 ± 0.7	373.6 ± 0.3	37

at each particular level and observing the resulting change in the retrieval. In a profile scaling retrieval, the rows of the averaging kernel matrix all have the shape of the a priori profile, and therefore the NxN matrix can be simplified to a N-vector, like that illustrated in Washenfelder et al. (2006).

Table 1 summarises the integrated aircraft and FTS average X_{CO2} during the upward and downward profiles. Unlike Washenfelder et al. (2006) we use the average CO_2 from the two bands, and do not previously scale the O_2 to a mean value of 0.2095. Rather than deriving separate CO_2 and O_2 corrections, one correction factor is used to cover the whole X_{CO_2} calculation. This results in identical calibrated X_{CO_2} numbers, but simplifies the calibration process. Ratioing the FTS and aircraft determinations of X_{CO_2} gives a correction factor of 0.988 ± 0.001 (mean $\pm$ standard deviation of the ratios of FTS to aircraft X_{CO2}). Aircraft campaigns over the Park Falls observatory resulted in correction factors of 0.991 ± 0.002 calculated in the same fashion as described above.

Using all aircraft overflights from both sites, the average correction factor is 0.990 ± 0.002. The FTS X_{CO_2} is therefore biased low by 1.0%. In the X_{CO_2} retrievals, the retrieved O_2 column is high by 2.3% (averaged over 260 000 spectra from Darwin and Park Falls), meaning the CO_2 column retrievals are approximately 1.3% higher than the in situ scale. This indicates an improvement with the updated spectroscopic line parameters relative to those used for the previous Park Falls analysis (Washenfelder et al., 2006). The improvement highlights the importance of line parameters to the accuracy of the retrieved FTS columns. Figure 7 shows all Park Falls and Darwin FTS-aircraft comparison points, and the best fit line illustrating the average TCCON correction factor. All points overlap with the best fit line within the calculated uncertainties, and the correction factors for Park Falls and Darwin agree with the average correction factor within uncertainties.

The method of calibration described here, and by Washenfelder et al. (2006) places the FTS measurements onto the same scale as the global in situ network. The calibration against aircraft profiles provides a transfer standard between TCCON sites, which will be valuable for future sites joining the network, especially those over which aircraft profiles will not be attained. Ideally timeseries of profiles would be obtained over all sites in order to correct for site-specific and time-varying instrument effects.

Table 2. Uncertainties in aircraft integrated columns sampling over specific altitude ranges.

Sampling range	Uncertainty in integrated X_{CO_2} ($\mu mol\,mol^{-1}$)
0–4 km	1.3
0–12 km	0.5
These flights	0.7
0.3–14.7 km (these flights w/no missing data)	0.4

8 Error discussion

In integrating the aircraft-based in situ measurements to create a calibrated column measurement we have made assumptions about approximately 20% of the profile. With the 2 $\mu mol\,mol^{-1}$ errors attributed to these points, they contribute more than 50% (0.4 out of 0.7 $\mu mol\,mol^{-1}$) of the error assigned to the integrated aircraft column. So the missing sections of the in situ profile (especially above the 139 hPa aircraft ceiling) dominate the derived column error. Table 2 summarizes the uncertainty in the column integrated X_{CO_2} over a variety of altitude sampling ranges compared to that obtained here. We now consider the effect of making different assumptions in assigning the upper and lower regions of the profile.

For the upper troposphere and stratosphere we compare the model results with two alternatives. Firstly, we take the alternative model results of Waugh et al. (1997) for the stratosphere, which showed a good match to previous aircraft measurements. The relationship between CO_2 and potential temperature in this modeled profile for the tropics during March–April is estimated to be $-0.0125\,\mu mol\,mol^{-1}\,K^{-1}$, and this gradient applied from the tropopause height upwards. The difference between the two integrated stratospheric profiles is 0.05 $\mu mol\,mol^{-1}$, considerably less than the assumed error of 0.18 $\mu mol\,mol^{-1}$ for this section of the profile.

We also compare our assumed upper profile with a composite case, consisting of aircraft profile measurements simultaneously acquired over Costa Rica during Costa Rica – Aura Validation Experiment (CR-AVE), which have shown a good match to the profiles during the TWP-ICE campaign from the TTL upwards (Park et al., 2007). The average profile measurement from this campaign is appended to the top of the profiles (above 360 K) used here, and then the original model assumption used to extend the stratospheric profile above the aircraft ceiling. The difference to the total integrated aircraft column dry-air mole fraction

for both profiles is 0.009 µmol mol^{-1}, and assuming an error of ± 0.1 µmol mol^{-1} for the WB57 values decreases the error estimate by ∼25%. The good agreement with the assumed model profile is heartening, and suggests that the ± 2 µmol mol^{-1} uncertainties attributed are indeed generous, and the assumptions are reasonable.

For the FTS X_{CO_2} columns, the magnitude of random errors is shown by the clear sky reproducibility of 0.1%. Due to spectroscopic errors, a systematic offset of 1% is introduced to the X_{CO_2} calculated from FTS measurements of vertical column CO_2 and O_2. These systematic errors are removed via correction to place the FTS determined X_{CO_2} on the WMO scale for low airmasses. Current spectroscopic linelists contain errors that cause apparent solar zenith angle dependence in the retrieved X_{CO_2} values; hence we apply an airmass-dependent correction to X_{CO_2} derived from data at Darwin and Park Falls. These errors may be due to missing lines, or in the line widths. We are confident that with several new spectroscopic measurements becoming available (Robichaud et al., 2008), the systematic errors in the O_2 and CO_2 columns and airmass dependencies can be significantly reduced.

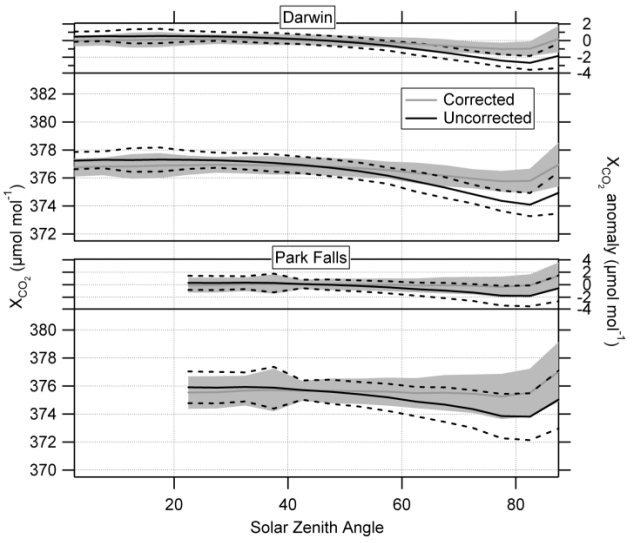

Fig. A1. X_{CO_2} and X_{CO_2} anomaly as a function of solar zenith angle for Darwin and Park Falls. The black line (the dashed lines show the standard deviation) in each panel is without the airmass correction applied, while the grey line and band are the airmass corrected values and their standard deviation.

9 Summary and conclusions

An automated solar observatory was deployed to Darwin, Australia, and has acquired near-infrared solar spectra since August 2005. The column CO_2 retrievals were calibrated using aircraft profiles collected over the site during the TWP-ICE campaign in January 2006. These profiles show the X_{CO_2} determined from FTS vertical column retrievals is underestimated by a factor of 0.988 ± 0.001, based on spectral fits using a modified HITRAN linelist. This bias is in reasonable agreement with that measured at Park Falls (0.991 ± 0.002), suggesting a common cause. The biases in the O_2 and CO_2 column retrievals result from inaccuracies in the spectroscopic line parameter database and the spectral fitting process.

The calibration described here presents a means of placing FTS column-average mole fractions from Darwin on to the same scale as in situ measurements. Data acquired from the site will assist in quantification of tropical CO_2 sources and sinks, where measurements are currently scarce. In addition, this site will provide validation of satellite measurements in this crucial region of the globe.

Appendix A

Airmass correction

There appears to be an airmass dependent artifact (ADA) in the retrieved X_{CO_2} values, not only for Darwin, but for all TCCON sites. The ADA causes X_{CO_2} retrievals to be approximately 1% larger at noon than sunrise or sunset, even at clean air sites and at times of the year when there is no physical reason for a diurnal change of X_{CO_2}. The ADA is aliased into the diurnal and seasonal cycles, causing systematic differences between sites. The aliasing problem is particularly important for Darwin and other Southern Hemisphere sites, where the seasonal cycle is smaller than in the Northern Hemisphere. The airmass dependency may be attributable to spectroscopic inadequacies, such as missing lines or errors in temperature-dependencies or line widths, or to instrumental problems such as zero level offsets, continuum curvature and ILS errors due to misalignment.

To derive and apply a correction for the ADA, we assume that on any given day, X_{CO_2} variation symmetrical about noon is an artifact, and anti-symmetric variation is real. This assumption should be reasonable for unpolluted sites, since the natural effect of photosynthesis and respiration is to cause a maximum X_{CO_2} at sunrise, and minimum at sunset. For each day, we represent the X_{CO_2} by three terms, a constant noon-time value ($\hat{y}$), a component varying symmetrically about noon ($S(\theta_i)$) and a component varying anti-symmetrically about noon ($A(\mathrm{t}_i)$). The amplitudes of each term are determined by a least-squares minimization of:

$$\chi^2 = \sum_i \left(\frac{X_{CO_2,i} - \hat{X}_{CO_2} - \alpha.A(t_i) - \beta.S(\theta_i)}{\varepsilon_i} \right) \quad \text{(A1)}$$

where:

$\hat{X}_{CO_2}$ = the noon X_{CO_2}

$X_{CO_2,i} \pm \varepsilon_{i,}$ = the retrieved X_{CO_2} and uncertainty for the ith spectrum

θ_i = the solar zenith angle for spectrum i (degrees)

t_i = the time at which the ith spectrum was acquired (in days)

t_{noon} = the time at local solar noon (in days)

$A(t_i) = \sin(2\pi(t_i - t_{\text{noon}}))$

$S(\theta_i) = \left(\frac{(\theta_i+13)}{(90+13)}\right)^3 - \left(\frac{(45+13)}{(90+13)}\right)^3$

$S(\theta_i)$ is defined to be zero at 45° because this minimizes the absolute size of the correction and it makes the $S(\theta_i)$ more orthogonal to $\hat{y}$, making the problem better posed mathematically. These basis function forms were determined from X_{CO_2} results from Darwin, which are the most plentiful of the TCCON sites, and cover the widest range of solar zenith angles. The decision was guided by the χ^2 of minimization. The X_{CO_2} can then be corrected using Eq. (A2).

$$X_{CO_2}^{\text{corrected}} = X_{CO_2} - \beta . S(\theta_i) \quad \text{(A2)}$$

An average value of beta of -0.0075 is determined using data from Park Falls and Darwin. Figure A1 shows the corrected (grey) and uncorrected (black) X_{CO_2} and X_{CO_2} anomaly as a function of solar zenith angle for Darwin and Park Falls. This value of beta results in a correction of -0.13% to X_{CO_2} at 0° solar zenith angle and 0.42% to X_{CO_2} at 80° solar zenith angle. The between-site and time-based variability in beta is around 10% of this figure, meaning that the potential bias introduced by applying the airmass correction is less than 0.05% in X_{CO_2}, significantly below the measurement reproducibility. The correction removes a large portion of the ADA. The consistency of the airmass-dependent correction between sites suggests that the spectroscopic factors contributing to the airmass-dependence are larger than the instrument specific factors.

Acknowledgements. We thank Rex Pearson, John Glowacki, Troy Culgan, Maciej Ryczek and Krzysztof Krzton for the maintenance of the solar FTS. We also gratefully acknowledge comments on the manuscript made by Janina Messerschmidt. Nicholas Deutscher is supported by an Australian Postgraduate Industry Award. The research described in this paper was performed for the Orbiting Carbon Observatory Project at the Jet Propulsion Laboratory, California Institute of Technology, under a contract with the National Aeronautics and Space Administration. TCCON is funded by the NASA terrestrial carbon cycle program, grant NNX08AI86G. This research is also assisted by Australian Research Council Projects DP0879468 and LP0562346 with the Australian Greenhouse Office.

Edited by: I. Aben

References

WMO/GAW Glossary of QA/QC-Related Terminology, WMO (2007), http://gaw.empa.ch/glossary.html, May 2010.

Andrews, A. E., Boering, K. A., Daube, B. C., Wofsy, S. C., Hintsa, E. J., Weinstock, E. M., and Bui, T. P.: Empirical age spectra for the lower tropical stratosphere from in situ observations of CO_2: Implications for stratospheric transport, J. Geophys. Res.-Atmos., 104, 26581–26595, 1999.

Andrews, A. E., Boering, K. A., Daube, B. C., Wofsy, S. C., Loewenstein, M., Jost, H., Podolske, J. R., Webster, C. R., Herman, R. L., Scott, D. C., Flesch, G. J., Moyer, E. J., Elkins, J. W.,Dutton, G. S., Hurst, D. F., Moore, F. L., Ray, E. A., Romashkin, P. A., and Strahan, S. E.: Mean ages of stratospheric air derived from in situ observations of CO_2, CH_4, and N_2O, J. Geophys. Res.-Atmos., 106, 32295–32314, 2001a.

Andrews, A. E., Boering, K. A., Wofsy, S. C., Daube, B. C., Jones, D. B., Alex, S., Loewenstein, M., Podolske, J. R., and Strahan, S. E.: Empirical age spectra for the midlatitude lower stratosphere from in situ observations of CO_2: Quantitative evidence for a subtropical "barrier" to horizontal transport, J. Geophys. Res.-Atmos., 106, 10257–10274, 2001b.

Boering, K. A., Wofsy, S. C., Daube, B. C., Schneider, H. R., Loewenstein, M., and Podolske, J. R.: Stratospheric mean ages and transport rates from observations of carbon dioxide and nitrous oxide, Science, 274, 1340–1343, 1996.

Bovensmann, H., Burrows, J. P., Buchwitz, M., Frerick, J., Noel, S., Rozanov, V. V., Chance, K. V., and Goede. A. P. H.: SCIAMACHY – mission objectives and measurement modes, J. Atmos. Sci., 56, 127–150, 1999.

Chevallier, F., Breon, F. M., and Rayner, P. J.: Contribution of the Orbiting Carbon Observatory to the estimation of CO_2 sources and sinks: Theoretical study in a variational data assimilation framework, J. Geophys. Res.-Atmos., 112, D09307, doi:10.1029/2006JD007375, 2007.

Crisp, D., Atlas, R. M., Breon, F.-M., Brown, L. R., Burrows, J. P., Ciais, P., Connor, B. J., Doney, S. C., Fung, I. Y., Jacob, D. J., Miller, C. E., O'Brien, D., Pawson, S., Randerson, J. T., Rayner, P. J., Salawitch, R. J., Sander, S. P., Sen, B., Stephens, G. L., Tans, P. P., Toon, G. C., Wennberg, P. O., Wofsy, S. C., Yung, Y. L., Kuang, Z., Chudasama, B., Sprague, G., Weiss, B., Pollock, R., Kenyon, D., and Schroll, S.: The Orbiting Carbon Observatory (OCO) Mission, Adv. Space Res., 34, 700–709, 2004.

Daube, B. C., Boering, K. A., Andrews, A. E., and Wofsy, S. C.: A high-precision fast-response airborne CO_2 analyzer for in situ sampling from the surface to the middle stratosphere, J. Atmos. Ocean. Tech., 19, 1532–1543, 2002.

Denning, A. S., Collatz, G. J., Zhang, C. G., Randall, D. A., Berry, J. A., Sellers, P. J., Colello, G. D., and Dazlich, D. A.: Simulations of terrestrial carbon metabolism and atmospheric CO_2 in a general circulation model. 1. Surface carbon fluxes, Tellus, 48B, 521–542, 1996.

Esler, M. B., Griffith, D. W. T., Wilson, S. R., and Steele, L. P.: Precision trace gas analysis by FTIR spectroscopy 1. Simultaneous analysis of CO_2, CH_4, N_2O and CO in air, Anal. Chem., 72, 206–215, 2000a.

Esler, M. B., Griffith, D. W. T., Wilson, S. R., and Steele, L. P.: Precision trace gas analysis by FTIR spectroscopy 2. The $^{13}C/^{12}C$ isotope ratio in CO_2, Anal. Chem., 72, 216–221, 2000b.

Forster, P., Ramaswamy, V., Artaxo, P., Berntsen, T., Betts, R., Fahey, D. W., Haywood, J., Lean, J., Lowe, D. C., Myhre, G., Nganga, J., Prinn, R., Raga, G., Schulz, M., and Dorland, R. V.: Changes in Atmospheric Constituents and in Radiative Forcing, in: Climate Change 2007: The Physical Science Basis. Contribution of Working Group I to the Fourth Assessment Report

of the Intergovernmental Panel on Climate Change, edited by: Solomon, S., Qin, D., Manning, M., Chen, Z., Marquis, M., Averyt, K. B., Tignor, M., and Miller, H. L., Cambridge University Press, Cambridge, UK and New York, NY, USA, 2007.

Frankenberg, C., Warneke, T., Butz, A., Aben, I., Hase, F., Spietz, P., and Brown, L. R.: Pressure broadening in the 2_v3 band of methane and its implication on atmospheric retrievals, Atmos. Chem. Phys., 8, 5061–5075, doi:10.5194/acp-8-5061-2008, 2008.

Gerbig, C., Körner, S., and Lin, J. C.: Vertical mixing in atmospheric tracer transport models: error characterization and propagation, Atmos. Chem. Phys., 8, 591–602, doi:10.5194/acp-8-591-2008, 2008.

GLOBALVIEW-CO_2: Cooperative Atmospheric Data Integration Project - Carbon Dioxide., CD-ROM, NOAA ESRL Boulder, Colorado, also available on Internet via anonymous FTP to ftp.cmdl.noaa.gov, Path: ccg/co2/GLOBALVIEW], 2008.

Gloor, M., Fan, S.-M., Pacala, S., and Sarmiento, J.: Optimal sampling of the atmosphere for purpose of inverse modeling: A model study, Global Biogeochem. Cy., 14, 407–428, 2000.

Gurney, K. R., Law, R. M., Denning, A. S., Rayner, P. J., Baker, D., Bousquet, P., Bruhwiler, L., Chen, Y. H., Ciais, P., Fan, S., Fung, I. Y., Gloor, M., Heimann, M., Higuchi, K., John, J., Maki, T., Maksyutov, S., Masarie, K., Peylin, P., Prather, M., Pak, B. C., Randerson, J., Sarmiento, J., Taguchi, S., Takahashi, T., and Yuen, C. W.: Towards robust regional estimates of CO_2 sources and sinks using atmospheric transport models, Nature, 415, 626–630, 2002.

Gurney, K. R., Law, R. M., Denning, A. S., Rayner, P. J., Baker, D., Bousquet, P., Bruhwiler, L., Chen, Y. H., Ciais, P. S., Fan, M., Fung, I. Y., Gloor, M., Heimann, M., Higuchi, K., John, J., Kowalczyk, E., Maki, T., Maksyutov, S., Peylin, P., Prather, M., Pak, B. C., Sarmiento, J., Taguchi, S., Takahashi, T., and Yuen, C. W.: TransCom 3 CO_2 inversion intercomparison: 1. Annual mean control results and sensitivity to transport and prior flux information, Tellus, 55B, 555–579, 2003.

Hume, T.: Radiation Dry Bias in TWP-ICE Radiosonde Soundings, paper presented at Seventeenth Atmospheric Radiation Measurement (ARM) Science Team Meeting, Monterey, California, 26–30 March 2007.

Inoue, G., Maksyutov, S. and THE GOSAT TEAM: Global carbon dioxide and methane column observation by GOSAT (Greenhouse gases observing satellite), Geophys. Res. Abstr., 8, 2006.

Kalnay, E., Kanamitsu, M., Kistler, R., Collins, W., Deaven, D., Gandin, L., Iredell, M., Saha, S., White, G., Woollen, J., Zhu, Y., Chelliah, M., Ebisuzaki, W., Higgins, W., Janowiak, J., Mo, K. C., Ropelewski, C., Wang, J., Leetmaa, A., Reynolds, R., Jenne, R., and Joseph, D.: The NCEP/NCAR 40-year reanalysis project, B. Am. Meteor. Soc., 77, 437–471, 1996.

Keppel-Aleks, G., Toon, G. C., Wennberg, P. O., and Deutscher, N. M.: Reducing the Impact of Source Brightness Fluctuations on spectra obtained by FTS, Appl. Optics, 46, 4774–4779, 2007.

Newman, S. M., Orr-Ewing, A. J., Newnham, D. A., and Ballard, J.: Temperature and pressure dependence of line widths and integrated absorption intensities for the O-2 a(1)Delta(g)-X-3 Sigma(-)(g) (0,0) transition, J. Phys. Chem., 104, 9467–9480, 2000.

Olsen, S. C. and Randerson, J. T.: Differences between surface and column atmospheric CO_2 and implications for carbon cycle research, J. Geophys. Res., 109, doi: 10.1029/2003JD003968, 2004.

Park, S., Jiménez, R., Daube, B. C., Pfister, L., Conway, T. J., Gottlieb, E. W., Chow, V. Y., Curran, D. J., Matross, D. M., Bright, A., Atlas, E. L., Bui, T. P., Gao, R.-S., Twohy, C. H., and Wofsy, S. C.: The CO2 tracer clock for the Tropical Tropopause Layer, Atmos. Chem. Phys., 7, 3989–4000, doi:10.5194/acp-7-3989-2007, 2007.

Paton-Walsh, C., Deutscher, N. M., Griffith, D. W. T., Forgan, B. W., Wilson, S. R., Jones, N. B., and Edwards, D. P.: Trace Gas Emissions from Savanna Fires in Northern Australia, J. Geophys. Res., doi:10.1029/2009JD013309, in press., 2010.

Rayner, P. J. and O'Brien, D. M.: The utility of remotely sensed CO_2 concentration data in surface source inversions, Geophys. Res. Lett., 28, 175–178, 2001.

Robichaud, D. J., Hodges, J. T., Brown, L. R., Lisak, D., Maslowski, P., Yeung, L. Y., Okumura, M., and Miller, C. E.: Experimental intensity and lineshape parameters of the oxygen *A*-band using frequency-stabilized cavity ring-down spectroscopy, J. Molec. Spec., 248, 1–13, 2008.

Rothman, L. S., Jacquemart, D., Barbe, A., Benner, D. C., Birk, M., Brown, L. R., Carleer, M. R., Chackerian, C., Chance, K., Coudert, L. H., Dana, V., Devi, V. M., Flaud, J. M., Gamache, R. R., Goldman, A., Hartmann, J. M., Jucks, K. W., Maki, A. G., Mandin, J. Y., Massie, S. T., Orphal, J., Perrin, A., Rinsland, C. P., Smith, M. A. H., Tennyson, J., Tolchenov, R. N., Toth, R. A., Vander Auwera, J., Varanasi, P., and Wagner, G.: The HITRAN 2004 molecular spectroscopic database, J. Quant. Spectrosc. Ra., 96, 139–204, 2005.

Smith, K. M. and Newnham, D. A.: Near-infrared absorption cross sections and integrated absorption intensities of molecular oxygen (O-2, O-2-O-2, and O-2-N-2), J. Geophys. Res., 105, 7383–7396, 2000.

Smith, K. M., Newnham, D. A., and Williams, R. G.: Collision-induced absorption of solar radiation in the atmosphere by molecular oxygen at 1.27 μm: Field observations and model calculations, J. Geophys. Res., 106, 7541–7552, 2001.

Tans, P. P., Zhao, C., and Masarie, K.: Maintenance and propagation of the WMO Mole Fraction Scale for carbon dioxide in air, in: Report of the Eleventh WMO Meeting of Experts on Carbon Dioxide Concentration and Related Tracer Measurement Techniques in Tokyo, Japan, 25–28 September 2001, edited by: Toru, S., World Meteorological Organization, Geneva, 2003.

Toth, R. A.: Measurements of positions, strengths and self-broadened widths of H_2O from 2900 to 8000 cm^{-1}: line strength analysis of the 2nd triad bands, J. Quant. Spectrosc. Ra., 94, 51–107, 2005.

Toth, R. A., Brown, L. R., Miller, C. E., Devi, V. M., and Benner, D. C.: Line strengths of (CO_2)-C-12-O-16: 4550–7000 cm(-1), J. Molec. Spec., 239, 221–242, 2006.

Toth, R. A., Miller, C. E., Brown, L. R., Malathy Devi, V., and Chris Benner, D.: Line positions and strengths of $^{16}O^{12}C^{18}O$, $^{18}O^{12}C^{18}O$ and $^{17}O^{12}C^{18}O$ between 2200 and 7000 cm^{-1}, J. Molec. Spec., 243, 43–61, 2007.

Vömel, H., David, D. E., and Smith, K.: Accuracy of Tropospheric and Stratospheric Water Vapor Measurements by the Cryogenic Frost Point Hygrometer (CFH): Instrumental Details and Observations, J. Geophys. Res., 112, doi:10.1029/2006JD007224, 2007a.

Vömel, H., Selkirk, H., Miloshevich, L., Valverde, J., Valdés, J., Kyrö, E., Kivi, R., Stolz, W., Peng, G., and Diaz, J. A.: Radiation dry bias of the Vaisala RS92 humidity sensor, J. Atmos. Ocean. Tech., 953–963, 24, 6, 2007b.

Washenfelder, R. A., Toon, G. C., Blavier, J. F., Yang, Z., Allen, N. T., Wennberg, P. O., Vay, S. A., Matross, D. M., and Daube, B. C.: Carbon dioxide column abundances at the Wisconsin Tall Tower site, J. Geophys. Res., 111, D22305, doi:10.1029/2006JD007154, 2006.

Waugh, D. W., Hall, T. M., Randel, W. J., Rasch, P. J., Boville, B. A., Boering, K. A., Wofsy, S. C., Daube, B. C., Elkins, J. W., Fahey, D. W., Dutton, G. S., Volk, C. M., and Vohralik, P. F.: Three-dimensional simulations of long-lived tracers using winds from MACCM2, J. Geophys. Res., 102, 21493–21513, 1997.

Wunch, D., Toon, G. C., Blavier, J.-F., Washenfelder, R. A., Notholt, J., Connor, B. J., Griffith, D. W. T., Sherlock, V., and Wennberg, P. O.: The Total Carbon Column Observing Network (TCCON), Philos. T. R. Soc. A, accepted, 2010a.

Wunch, D., Toon, G. C., Wennberg, P. O., Wofsy, S. C., Stephens, B. B., Fischer, M. L., Uchino, O., Abshire, J. B., Bernath, P., Biraud, S. C., Blavier, J.-F. L., Boone, C., Bowman, K. P., Browell, E. V., Campos, T., Connor, B. J., Daube, B. C., Deutscher, N. M., Diao, M., Elkins, J. W., Gerbig, C., Gottlieb, E., Griffith, D. W. T., Hurst, D. F., Jiménez, R., Keppel-Aleks, G., Kort, E., Macatangay, R., Machida, T., Matsueda, H., Moore, F., Morino, I., Park, S., Robinson, J., Roehl, C. M., Sawa, Y., Sherlock, V., Sweeney, C., Tanaka, T., and Zondlo, M. A.: Calibration of the total carbon column observing network using aircraft profile data, Atmos. Meas. Tech. Discuss., 3, 2603–2632, doi:10.5194/amtd-3-2603-2010, 2010b.

Yang, Z., Wennberg, P. O., Cageao, R. P., Pongetti, T. J., Toon, G. C., and Sander, S. P.: Ground-based photon path measurements from solar absorption spectra of the O_2 A-band, J. Quant. Spectrosc. Ra., 90, 309–321, 2005.